CATANet: Efficient Content-Aware Token Aggregation for Lightweight Image Super-Resolution

Xin Liu   Jie Liu$^{\boxtimes}$ Jie Tang   Gangshan Wu

State Key Laboratory for Novel Software Technology, Nanjing University, Nanjing 210023, China

xinliu2023@smail.nju.edu.cn   {liujie,tangjie,gswu}@nju.edu.cn

https://github.com/EquationWalker/CATANet

Abstract

*Transformer-based methods have demonstrated impressive performance in low-level visual tasks such as Image Super-Resolution (SR). However, its computational complexity grows quadratically with the spatial resolution. A series of works attempt to alleviate this problem by dividing Low-Resolution images into local windows, axial stripes, or dilated windows. SR typically leverages the redundancy of images for reconstruction, and this redundancy appears not only in local regions but also in long-range regions. However, these methods limit attention computation to content-agnostic local regions, limiting directly the ability of attention to capture long-range dependency. To address these issues, we propose a lightweight Content-Aware Token Aggregation Network (CATANet). Specifically, we propose an efficient Content-Aware Token Aggregation module for aggregating long-range content-similar tokens, which shares token centers across all image tokens and updates them only during the training phase. Then we utilize intra-group self-attention to enable long-range information interaction. Moreover, we design an inter-group cross-attention to further enhance global information interaction. The experimental results show that, compared with the state-of-the-art cluster-based method SPIN, our method achieves superior performance, with a maximum PSNR improvement of 0.33dB and nearly **double** the inference speed.*

1. Introduction

Single Image Super-Resolution (SISR) is a classic task in computer vision and image processing. Its goal is to recover High-Resolution (HR) images from its Low-Resolution (LR) counterpart. SISR is widely applied in various fields, such as medical imaging, digital photography, and reducing server costs for streaming media transmission.

Since the pioneering work of Convolutional Neural Networks (CNNs) in SISR [9], numerous CNN-based meth-
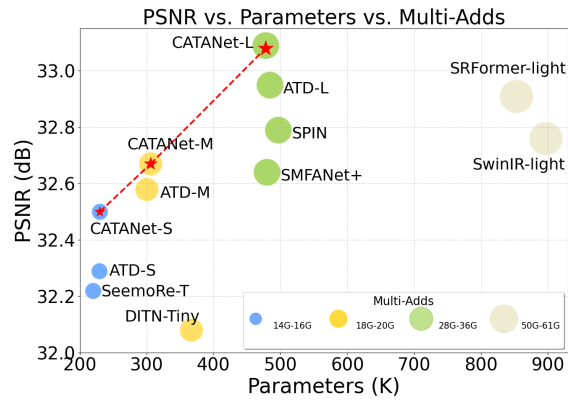

Figure 1. Performance and model complexity comparison on Urban100 dataset for upscaling factor ×2.

ods [10, 20–22, 25, 58, 61] have been proposed to challenge the reconstruction of HR images from LR images. Due to the local mechanism of convolution, which limits the capture of global dependencies, some CNN-based methods [25, 61] use very deep and complex network architectures to increase receptive fields and achieve better performance. However, these methods inevitably increase computational resources, which restricts their applicability.

Recently, with the success of transformers in NLP [42], transformers have been applied to multiple high-level computer vision tasks [3, 8, 12, 31, 46], achieving remarkable results. The key success of transformer-based approaches is the Self-Attention mechanism, which can effectively capture long-range dependencies. Due to the powerful potential of transformers, they have also attracted attention in low-level computer vision tasks [4, 5, 24, 45, 50, 53, 59], including image super-resolution. HAT [4] shows through experiments that utilizing more global information can effectively enhance the quality of reconstructed images. However, these methods divide larger images into smaller local regions for separate processing to alleviate the high complexity of global self-attention. Although this strategy can improve the efficiency of transformer-based models and pro-

---

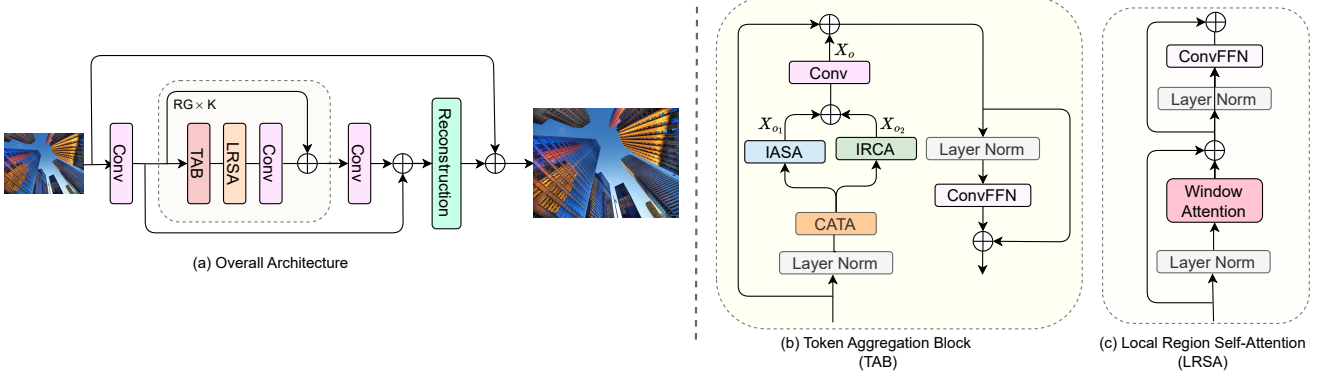$^{\boxtimes}$: Corresponding author (liujie@nju.edu.cn).

1

Figure 2. The overall architecture of CATANet and the structure of Token Aggregation Block and Local-Region Self-Attenion.

vide more refined local information, it still has some limitations. SwinIR [24] divides the image into content-agnostic local windows, limiting the use of similar tokens over long ranges and resulting in undesirable results. Axial stripe attention [11] expands the receptive field in a cross-shaped pattern, but this approach remains content-agnostic and may introduce some irrelevant interfering information.

To alleviate these issues, some methods have explored clustering-based solutions. SPIN [56], for instance, employs the soft k-means-based token algorithm [19] for clustering, using the cluster centers as proxies between query and key in the attention mechanism, facilitating the propagation of long-range information. However, SPIN still encounters two primary limitations: (1) The cluster centers provide a sparse representation of the image tokens. However, relying exclusively on these centers for long-range information propagation results in a coarse approximation, which is insufficient for capturing and leveraging detailed long-range dependencies. (2) The inference speed of SPIN is limited due to the need for iterative processing over clustering centers during inference, which constrains the deployment of lightweight models. ATD [57] introduces an auxiliary dictionary to learn priors from the training data and uses the dictionary to classify tokens, leading to more accurate token grouping. However, ATD applies multiple attention mechanisms concurrently to boost performance, which significantly increases computational burden and makes ATD less suitable for lightweight scenarios, as shown in Fig.1.

To address these challenges, we propose a novel efficient Content-Aware Token Aggregation Network (CATANet) with Token-Aggregation Block as its core component. Token-Aggregation Block mainly consists of efficient Content-Aware Token Aggregation module, Intra-Group Self-Attention, and Inter-Group Cross-Attention. In contrast to the clustering methods previously discussed, we designed an efficient token centers updating strategy within our Content-Aware Token Aggregation (CATA) module. It shares token centers across all image tokens and updates them only during the training phase, eliminating the impact

of updating token centers on model inference speed. Unlike SPIN [56], which uses clustering centers for long-range information propagation, our Intra-Group Self-Attention employs CATA module to efficiently aggregate content-similar tokens together, forming content-aware regions. Attention is performed within each group, allowing for finer-grained long-range interactions among token information. Moreover, we introduce Inter-Group Cross-Attention, which applies cross-attention between each group and token centers, further enhancing global information interaction.

In summary, our main contributions are as follows:
• We propose a novel lightweight image SR network, Content-Aware Token Aggregation Network (CATANet). Our CATANet combines token aggregation with attention mechanisms to capture long-range dependencies while ensuring high inference efficiency.
• To mitigate the impact of token centers updates on inference speed, we designed efficient Content-Aware Token Aggregation (CATA) that only updates the token centers during the training phase.
• We propose Intra-Group Self-Attention and Inter-Group Cross-Attention, which operate between tokens and effectively capture long-range and global dependencies, effectively reduce interference from irrelevant information, and achieve computational complexity comparable to local-region-based methods.
• We conducted extensive experiments to demonstrate that our method surpasses the state-of-the-art cluster-based lightweight SR method SPIN, with a maximum PSNR improvement of 0.33 dB and nearly double the inference speed.

2. Related Work

Deep Networks for SR. Deep neural networks have become the mainstream solutions for Image Super-Resolution in recent years due to their powerful representation learning capabilities. Since SRCNN [9] first successfully applied CNNs to the SR field through a three-layer CNN network, a large number of CNN-based methods have achieved
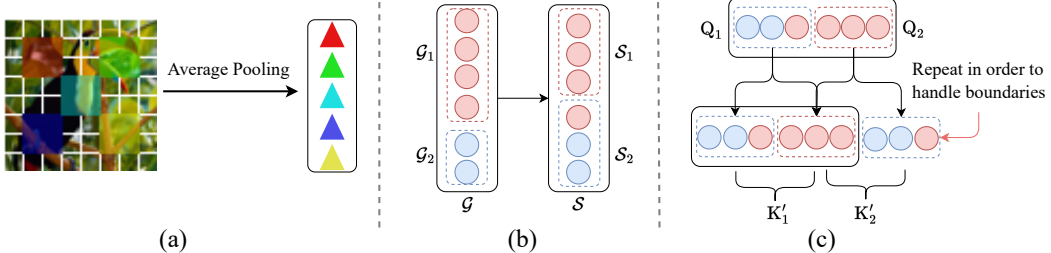
Figure 3. (a) A simple illustration for obtaining the initial token centers. (b) Visualization of sub-grouping. The dashed boxes of the same color indicate the same group (left) or subgroup (right). (c) Each subgroup's $\mathbf{Q}_j$ to attend to the $\mathbf{K}_j$ of two consecutive subgroups, where the same color denotes the same group $\mathcal{G}_j$

state-of-the-art performance using more complex or efficient structures, such as those with residual connections [25, 27, 47, 61] and U-shaped architectures [7, 29, 34]. Compared to CNNs, attention mechanisms have better long-range modeling capabilities, so attention mechanisms have also been introduced into SR to extract the most important features over long ranges. For example, RACN [60] utilizes channel attention, while CSFM [15] and DAT [6] combines spatial and channel attention. Recently, a series of transformer-based methods have been proposed and have refreshed the state-of-the-art (SOTA), demonstrating the powerful representation learning ability of transformers. For example, SwinIR [24] applies the Swin Transformer [31] framework to SR by dividing the entire image into small windows of size 8×8 and shifting the windows when applying multi-head attention mechanisms. Although the above methods can efficiently extract informative features, they often require a large number of parameters.

Lightweight Super-Resolution Methods. Due to the urgent demands for applying networks to resource-constrained devices, lightweight SR has attracted widespread attention[9, 23, 39, 52, 62]. For example, ESPCN [9] and FSRCNN [39] utilize post-upsampling techniques to reduce computational costs. IDN [17] and IMDN [18] employ information distillation blocks to extract useful information, dividing the input features into two streams using slicing operations, with one stream further enhancing feature representation through convolution. Subsequently, the two features are combined to obtain richer information. For lightweight super-resolution based on transformers, most methods focus on sparse attention mechanisms, such as window-based attention [24] and group-wise attention [59], to reduce the high computational complexity of attention calculation. Although these methods effectively reduce computational complexity, their sparse nature is content-agnostic and cannot guarantee the quality of SR reconstruction.

Token Clustering for Computer Vision. Token clustering is a well-studied task in computer vision, and recent advances in deep learning have made significant progress in this area. A common approach is to use traditional clus-

tering algorithms, such as k-means, to gather similar tokens together. For example, BOAT [51] employs hierarchical clustering to gather similar tokens together and computes attention within each cluster. SPIN [56] utilizes the soft k-means-based token algorithm [19] to aggregate tokens, using the aggregated tokens as proxies between Query and Key to leverage long-range information. Although these token clustering methods have shown promising results in computer vision, the computational cost of the clustering process is significant, which hinders the application of token clustering in lightweight SR.

3. Method

3.1. Network Architecture

The overall network of the proposed CATANet comprises three modules: shallow feature extraction, deep feature extraction, and image reconstruction, as illustrated in Fig. 2(a). The shallow feature extraction is performed by a 3×3 convolutional layer, which maps the image from the original input space to a high-dimensional feature space. Let $\mathbf{I}_{\mathrm{LR}}$ and $\mathbf{I}_{\mathrm{SR}}$ represent the Low-Resolution (LR) input image and the Super-Resolved (SR) image, respectively. We first get shallow feature $\mathbf{X}_0$ by

$$\mathbf{X}_0 = \mathrm{F}_{\mathrm{S}}(\mathbf{I}_{\mathrm{LR}}),$$

where F_{S} denotes the function of the shallow feature extraction. Then deeper features are extracted by sequential Residual Group (RG) of K. Each RG includes three components: Token-Aggregation Block (TAB), Local-Region Self-Attention (LRSA), and 3×3 convolution (Conv).

The input features of each RG are first processed through a TAB module to perform token aggregation, capturing long-range dependencies. Then, we use a LRSA to enhance the dependencies between tokens in local regions. Furthermore, we employ a 3×3 convolution at the end of each RG to further refine local features and implicitly learn positional embedding. Formally, for the i-th RG, the whole process can be formulated as:

$$\mathbf{X}_i = \mathbf{X}_{i-1} + \mathrm{F}_{\mathrm{Conv}}\left(\mathrm{F}_{\mathrm{LRSA}}\left(\mathrm{F}_{\mathrm{TAB}}\left(\mathbf{X}_{i-1}\right)\right)\right),$$

3

where $\mathbf{X}_i$ denotes the output feature in the i-th RG and $\mathrm{F}(\cdot)$ denotes the function of each individual component. Following previous work [24, 27], residual connections are used to stabilize the training process.

After K RGs, we use the image reconstruction module to obtain global residual information, which is then added to the upsampled image of $\mathbf{I}_{\mathrm{LR}}$ to obtain the high-resolution image $\mathbf{I}_{\mathrm{SR}}$.

$$\mathbf{I}_{\mathrm{SR}} = \mathrm{F}_{\mathrm{Up}}(\mathbf{I}_{\mathrm{LR}}) + \mathrm{F}_{\mathrm{IR}}(\mathbf{X}_K),$$

where F_{Up} denotes the function of the upsampling operator and F_{IR} denotes the function of the image reconstruction that includes a 3×3 convolution and a pixel shuffle [39].

3.2. Token-Aggregation Block (TAB)

In previous token clustering-based methods, BOAT [51] proposed a hierarchical clustering-based attention mechanism to achieve fine-grained long-range information interaction. However, the hierarchical clustering requires iterative updates of cluster centroids, slowing down model inference. SPIN [56] uses cluster centers as proxies between Query and Key in self-attention, facilitating long-range information propagation. This method, though, results in coarse information transmission, inevitably introducing irrelevant information. In contrast, we propose Intra-Group Self-Attention to achieve more refined information interaction between content-similar tokens. Moreover, like BOAT, SPIN suffers from slow inference speed.

To address these issues more effectively, we propose Token-Aggregation Block (TAB). As shown in Fig. 2(b), TAB mainly consists of four parts: Content-Aware Token Aggregation module, Intra-Group Self-Attention, Inter-Group Cross-Attention and a 1×1 convolution. By utilizing these four modules, we can efficiently achieve fine-grained long-range information interaction while allowing us to enjoy computational complexity similar to local-region attention.

3.2.1. Content-Aware Token Aggregation (CATA)

The process of CATA module is illustrated in Algorithm 1, where $\mathcal{M}$ is the cosine similarity function. As shown in Fig. 3(a), we obtain the initial M token centers $\{c_j\}_{j=1\cdots M}$ by simply performing average pooling over regular regions. Inspired by Routing Transformer [38], we share token centers among all image tokens, aiming to learn a set of global token centers across the training dataset rather than for each individual image. We update token centers using Exponential Moving Average (EMA), with a decay parameter λ typically set to 0.999.

Image tokens are divided into M content-similar token groups based on the similarity between each token and the token centers. A visualized example of the CATA module is shown in Fig. 4, where it can be seen that our token groups

---

Algorithm 1 Content-Aware Token Aggregation

▷ **input :** image tokens $\mathbf{X} = \{x_i \in \mathbb{R}^d\}_{i=1\cdots N}$
▷ **input :** token centers $\mathbf{C} = \{c_j \in \mathbb{R}^d\}_{j=1\cdots M}$
▷ **output :** token groups $\{\mathcal{G}_j\}_{j=1\cdots M}$

1: **if not training then**
2:     **go to** 13
3: **end if**
4: $\{c'_j\} = \{c_j\}$
5: **for** $t = T, \ldots, 1$ **do**
6:     // the similarity between tokens and token centers.
7:     $\mathbf{D} = \mathcal{M}(\{x_i\}, \{c'_j\})$ // $\mathbf{D} \in \mathbb{R}^{N \times M}$
8:     $\{\mathcal{G}_j\} = \left\{\{x^i \,\big|\, \arg\max_k \mathbf{D}_{ik} = j\}\right\}$
9:     $\{c'_j\} = \left\{\frac{1}{|\mathcal{G}_j|} \sum_{k=1}^{|\mathcal{G}_j|} x_k \,\big|\, x_k \in \mathcal{G}_j\right\}$
10: **end for**
11: // Update token centers using EMA.
12: $\{c_j\} = \{\lambda \cdot c_j + (1-\lambda) \cdot c'_j\}$
13: $\mathbf{D} = \mathcal{M}(\{x_i\}, \{c_j\})$
14: $\{\mathcal{G}_j\} = \left\{\{x^i \,\big|\, \arg\max_k \mathbf{D}_{ik} = j\}\right\}$

Table 1. Ablation study attending to consecutive subgroups. PSNR are calculated with a scale factor of 4.

Method	Params	Multi-Adds	Urban100	Manga109
Not Attend	536K	46.8G	26.85	31.26
Attend (ours)	536K	46.8G	26.87	31.31

aggregate content-similar tokens over long ranges, resulting in more precise token grouping. However, the number of tokens in each group may differ, which results in low parallelism efficiency. To address the issue of unbalanced group, as shown in Fig. 3(b), we refer to [37] to further divide the groups $\mathcal{G}$ into subgroups $\mathcal{S}$:

$$\mathcal{G} = \left[\mathcal{G}_1^1, \mathcal{G}_1^2 \cdots, \mathcal{G}_1^{n_1}, \cdots, \mathcal{G}_M^{n_M}\right],$$
$$\mathcal{S}_j = \left[\mathcal{G}_{j*g_s+1}, \mathcal{G}_{j*g_s+2}, \cdots, \mathcal{G}_{(j+1)*g_s}\right],$$
$$\mathcal{S} = [\mathcal{S}_1, \mathcal{S}_2, \cdots, \mathcal{S}_j, \cdots],$$

where the group $\mathcal{G}_i$ contains n_i tokens. Each group is concatenated to form $\mathcal{G}$, then divided into subgroups $\mathcal{S}$. After division, all subgroups have the same fixed size g_s, improving parallelism efficiency. As shown in Tab. 6(last two rows), by utilizing sub-grouping, the inference speed of CATANet is approximately doubled.

3.2.2. Intra-Group Self-Attention (IASA)

Given the subgroups $\mathcal{S} = \{\mathcal{S}_j\}$, we project it into matrix $\{\mathbf{Q}_j\}$, $\{\mathbf{K}_j\}$, and $\{\mathbf{V}_j\}$, as follows:

$$\mathbf{Q}_j, \mathbf{K}_j, \mathbf{V}_j = \mathcal{S}_j\mathbf{W}^Q, \mathcal{S}_j\mathbf{W}^K, \mathcal{S}_j\mathbf{W}^V,$$

where $\mathbf{W}^Q, \mathbf{W}^K$ and $\mathbf{W}^V \in \mathbb{R}^{d\times d}$ are weight matrices. To enhance parallel efficiency, we divide the groups $\mathcal{G}$ into sub-groups $\mathcal{S}$. However, this may result in content-similar tokens being split into adjacent subgroups. To mitigate this issue, we allow each subgroup's $\mathbf{Q}_j$ to attend to the $\mathbf{K}_j$ of
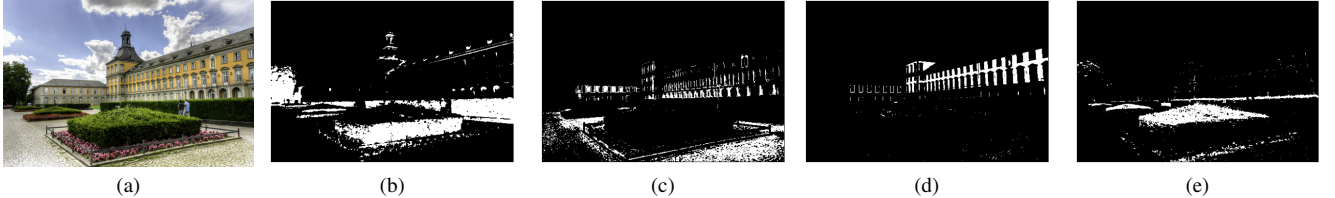
Figure 4. Visualization of token grouping results of TAB. (a) is the input image. The white part of each binarized image from (b) - (e) represents a single token group $\mathcal{G}_j$.

two consecutive subgroups, as shown in Fig.3(c). Furthermore, as shown in Tab. 1, attending to adjacent subgroups effectively enhances performance without adding computational overhead. The procedure can be formulated as:

$$
\begin{aligned}
\mathbf{K}'_j &= [\mathbf{K}_j, \mathbf{K}_{j+1}], \mathbf{V}'_j = [\mathbf{V}_j, \mathbf{V}_{j+1}], \\
\mathbf{O}_j &= \text{MSA}\left(\mathbf{Q}_j, \mathbf{K}'_j, \mathbf{V}'_j\right), \\
\mathbf{X}_{o_1} &= \text{PushBack}\left(\{\mathbf{O}_j\}\right),
\end{aligned}
\tag{1}
$$

where $\text{MSA}(\cdot)$ denotes Multi-Head Self-Attention operation [42] and PushBack operation put each token back to its original position on the feature map to form $\mathbf{X}_{o_1}$.

3.2.3. Inter-Group Cross-Attention (IRCA)

As shown in Algorithm 1, during the training phase, the token centers $\mathbf{C}$ aggregate content-similar tokens, summarizing global prior information. To leverage this global prior, we perform cross-attention between each subgroup $\mathcal{S}_j \in \mathbb{R}^{g_s \times d}$ and $\mathbf{C} \in \mathbb{R}^{M \times d}$, as follows:

$$
\begin{aligned}
\mathbf{O}'_j &= \text{MSA}\left(\mathcal{S}_j \mathbf{W}^q, \mathbf{C}\mathbf{W}^k, \mathbf{C}\mathbf{W}^v\right), \\
\mathbf{X}_{o_2} &= \text{PushBack}\left(\{\mathbf{O}'_j\}\right),
\end{aligned}
$$

where $\mathbf{W}^q, \mathbf{W}^k$ and $\mathbf{W}^v \in \mathbb{R}^{d \times d}$ are weight matrices. We set $M \ll N$ to maintain a low computational cost. Finally, $\mathbf{X}_o$ is obtained by fusing $\mathbf{X}_{o_2}$ and $\mathbf{X}_{o_1}$ from Eq. (1) through a convolution:

$$
\mathbf{X}_o = \text{F}_{\text{Conv}}\left(\mathbf{X}_{o_1} + \mathbf{X}_{o_2}\right).
$$

3.3. Local-Region Self-Attention (LRSA)

As shown in Fig. 2(c), the LASA follows HPINet [28], using overlapping patches to enhance feature interaction LRSA module is responsible for learning finer local details. Given input $\mathbf{X}_o \in \mathbb{R}^{N \times d}$, this process can be expressed as:

$$
\mathbf{X}_{out} = \text{MSA}(\mathbf{X}_o \mathbf{W}_Q, \mathbf{X}_o \mathbf{W}_K, \mathbf{X}_o \mathbf{W}_V),
$$

where $\mathbf{X}_{out} \in \mathbb{R}^{N \times d}$. $\mathbf{W}_Q, \mathbf{W}_K$ and $\mathbf{W}_V$ are weight matrices that are shared across patches.

ConvFNN. Similar to the Transformer layer, after TAB and LRSA, ConvFNN [64] is employed to perform feature interactions along the channel dimension, as illustrated in Fig. 2. Additionally, layer normalization is added before the TAB, LRSA, and ConvFNN, and residual shortcuts after both modules are added as well.

4. Experiments

4.1. Experimental Settings

We train the model using DIV2K [41], a high-quality dataset widely used for SR tasks. It includes 800 training images together with 100 validation images. Additionally, we evaluate our model on five commonly used public super-resolution datasets, including Set5 [2], Set14 [55], B100 [35], Urban100 [16], and Manga109 [36].

We use the metrics PSNR and SSIM [49] to evaluate our model performance. Following previous work [24, 64], both metrics are first transformed into the YCbCr color space and then computed on the Y channel. Details of the training procedure and network hyperparameters can be found in the supplementary material.

4.2. Comparisons with the state-of-the-arts

We compare the proposed CATANet with commonly used lightweight SR models for scaling factors ×2, ×3, and ×4, including CNN-based models (CRAN [1], LatticeNet [33], IMDN [18], RFDN [27], AWSRAN-M [44], and OSFFNet [48]) and transformer-based models (ESRT [32], ELAN-light [59], A-CubeNet [14], SwinIR [24], and SPIN [56]). Tab. 2 shows the quantitative comparison results of our model and other models in terms of PSNR and SSIM. As shown, our CATANet outperforms the compared methods on all benchmark datasets with three factors. Meanwhile, we have 15K fewer parameters compared to SPIN. It is notable that, thanks to the more refined long-range information interaction, our CATANet† outperforms SPIN by a maximum PSNR of 0.60dB, which is a significant improvement in image SR. Even without self-ensemble, our CATANet still surpass SPIN with a PSNR improvement of 0.33 dB. Additionally, we conduct a more comprehensive and fair comparison with more state-of-the-art methods in Sec. 4.5.

Visual Comparison. We provide some visual examples using different methods in Fig. 6. Compared to other methods, our CATANet can accurately restore clean edges with fewer artifacts because it captures similar textures from long ranges to supplement more long-range information, which indicates the superiority of our method. More visual examples can be found in the supplementary material.

5

Table 2. Comparison (PSNR/SSIM) with SOTA methods for image SR. Best and second best results are colored with red and blue. †
indicate that self-ensemble strategy [26] is used in testing.

Method	Scale	Params	Set5		Set14		B100		Urban100		Manga109	
			PSNR	SSIM	PSNR	SSIM	PSNR	SSIM	PSNR	SSIM	PSNR	SSIM
CARN [1]	×2	1592K	37.76	0.9590	33.52	0.9166	32.09	0.8978	31.92	0.9256	38.36	0.9765
IMDN [18]	×2	694K	38.00	0.9605	33.63	0.9177	32.19	0.8996	32.17	0.9283	38.88	0.9774
RFDN [27]	×2	530K	38.05	0.9606	33.68	0.9184	32.16	0.8994	32.12	0.9278	38.88	0.9773
AWSRAN-M [44]	×2	1063K	38.04	0.9605	33.66	0.9181	32.21	0.9000	32.23	0.9294	38.66	0.9772
OSFFNet [48]	×2	516K	38.11	0.9610	33.72	0.9190	32.29	0.9012	32.67	0.9331	39.09	0.9780
ESRT [32]	×2	677K	38.03	0.9600	33.75	0.9184	32.25	0.9001	32.58	0.9318	39.12	0.9774
ELAN-light [59]	×2	582K	38.17	0.9611	33.94	0.9207	32.30	0.9012	32.76	0.9340	39.11	0.9782
A-CubeNet [14]	×2	1380K	38.12	0.9609	33.73	0.9191	32.26	0.9007	32.39	0.9308	38.88	0.9776
SwinIR-light [24]	×2	878K	38.14	0.9611	33.86	0.9206	32.31	0.9012	32.76	0.9340	39.12	0.9783
SPIN [56]	×2	497K	38.20	0.9615	33.90	0.9215	32.31	0.9015	32.79	0.9340	39.18	0.9784
CATANet (ours)	×2	477K	38.28	0.9617	33.99	0.9217	32.37	0.9023	33.09	0.9372	39.37	0.9784
CATANet† (ours)	×2	477K	38.35	0.9620	34.11	0.9229	32.41	0.9027	33.33	0.9387	39.57	0.9788
CARN [1]	×3	1592K	34.29	0.9255	30.29	0.8407	29.06	0.8034	28.06	0.8493	33.43	0.9427
IMDN [18]	×3	703K	34.36	0.9270	30.32	0.8417	29.09	0.8046	28.17	0.8519	33.61	0.9445
RFDN [27]	×3	540K	34.41	0.9273	30.34	0.8420	29.09	0.8050	28.21	0.8525	33.67	0.9449
AWSRAN-M [44]	×3	1143K	34.42	0.9275	30.32	0.8419	29.13	0.8059	28.26	0.8545	33.64	0.9450
OSFFNet [48]	×3	524K	34.58	0.9287	30.48	0.8450	29.21	0.8080	28.49	0.8595	34.00	0.9472
ESRT [32]	×3	770K	34.42	0.9268	30.43	0.8433	29.15	0.8063	28.46	0.8574	33.95	0.9455
ELAN-light [59]	×3	590K	34.64	0.9288	30.55	0.8463	29.21	0.8081	28.69	0.8624	34.00	0.9478
A-CubeNet [14]	×3	1560K	34.53	0.9281	30.45	0.8441	29.17	0.8068	28.38	0.8568	33.90	0.9466
SwinIR-light [24]	×3	886K	34.62	0.9289	30.54	0.8463	29.20	0.8082	28.66	0.8624	33.98	0.9478
SPIN [56]	×3	569K	34.65	0.9293	30.57	0.8464	29.23	0.8089	28.71	0.8627	34.24	0.9489
CATANet (ours)	×3	550K	34.75	0.9300	30.67	0.8481	29.28	0.8101	29.04	0.8689	34.40	0.9499
CATANet† (ours)	×3	550K	34.83	0.9307	30.73	0.8490	29.34	0.8111	29.24	0.8718	34.69	0.9512
CARN [1]	×4	1592K	32.13	0.8937	28.60	0.7806	27.58	0.7349	26.07	0.7837	30.42	0.9070
IMDN [18]	×4	715K	32.21	0.8948	28.58	0.7811	27.56	0.7353	26.04	0.7838	30.45	0.9075
RFDN [27]	×4	550K	32.24	0.8952	28.61	0.7819	27.57	0.7360	26.11	0.7858	30.58	0.9089
AWSRAN-M [44]	×4	1520K	32.32	0.8969	28.72	0.7847	27.65	0.7382	26.27	0.7913	30.81	0.9114
OSFFNet [48]	×4	537K	32.39	0.8976	28.75	0.7852	27.66	0.7393	26.36	0.7950	30.84	0.9125
ESRT [32]	×4	751K	32.19	0.8947	28.69	0.7833	27.69	0.7379	26.39	0.7962	30.75	0.9100
ELAN-light [59]	×4	601K	32.43	0.8975	28.78	0.7858	27.69	0.7406	26.54	0.7982	30.92	0.9150
A-CubeNet [14]	×4	1520K	32.32	0.8969	28.72	0.7847	27.65	0.7382	26.27	0.7913	30.81	0.9114
SwinIR-light [24]	×4	897K	32.44	0.8976	28.77	0.7858	27.69	0.7406	26.47	0.7980	30.92	0.9151
SPIN [56]	×4	555K	32.48	0.8983	28.80	0.7862	27.70	0.7415	26.55	0.7998	30.98	0.9156
CATANet (ours)	×4	535K	32.58	0.8998	28.90	0.7880	27.75	0.7427	26.87	0.8081	31.31	0.9183
CATANet† (ours)	×4	535K	32.68	0.9009	28.98	0.7894	27.80	0.7437	27.04	0.8113	31.58	0.9206

Table 3. Ablation Study on IASA and IRCA. PSNR are calculated with a scale factor of 4.

IASA	IRCA	Params	Multi-Adds	Set5	Set14	B100	Urban100	Manga109
✗	✗	366K	37.3G	32.26	28.63	27.68	26.46	30.81
✓	✗	511K	46.8G	32.47	28.75	27.75	26.85	31.24
✓	✓	535K	46.8G	32.58	28.90	27.75	26.87	31.31

Table 4. Ablation Study on different designs of TAB. PSNR are calculated with a scale factor of 2.

Method	Set5	Set14	B100	Urban100	Manga109
Clustered Attention [43]	32.25	33.84	32.33	32.96	39.30
TCformer [54]	38.06	33.87	32.32	32.90	39.17
NLSA [37]	37.67	33.29	31.96	31.22	37.78
CATANet (ours)	38.28	33.99	32.37	33.09	39.37

Table 5. Ablation Study on fusion approach of IASA and IRCA. PSNR are calculated with a scale factor of 4.

Method	Params	Multi-Adds	Set5	Urban100	Manga109
concat	548K	47.6G	32.49	26.82	31.28
add (ours)	535K	46.8G	32.58	26.87	31.31

4.3. Ablation Study

In this section, we conduct ablation studies to better understand and evaluate each component in the proposed CATANet. For a fair comparison, we implemented all experiments based on ×4 CATANet and trained them un-

der the same settings. Besides, we set the input size as $3 \times 256 \times 256$ to compute Multi-Adds.

Effects of IASA and IRCA. The **I**ntra-**G**roup **S**elf-**A**ttention (IASA) and **I**nter-**G**roup **C**ross-**A**ttention (IRCA) is a core component of CATANet to capture long-range dependencies for recovering damaged images. To evaluate the effectiveness of the proposed modules, we establish three models and compare their ability for image SR. *The first model (row 1)* is the baseline model; we remove TAB and only adopt LRSA to process image features. To demonstrate the effectiveness of IASA, we propose *the second model (row 2)* that includes an additional IASA branch on top of the first model. In *the third model (row 3)*, we employ both IASA and IRCA simultaneously to show that IRCA can further enhance the utilization of long-range information. As shown in Tab. 3, we can observe that with the help of IASA, *the second model (row 2)* has a significant improvement on most datasets compared to *the first model (row 1)*, with a maximum improvement of 0.17dB. With the joint help of IASA and IRCA, *the third model (row 3)* once again has a significant improvement in all five datasets

compared to *the second model (row 2)*, with a maximum increase of 0.15dB. These are notable boosts in lightweight image SR.

Effects of different designs of TAB. To evaluate the effectiveness of our proposed Token Aggregation Block (TAB), we compare it with several other token aggregation methods in Tab. 4. Specifically, the Clustered Attention [43] replaces $\mathbf{Q}$ in standard attention with cluster centers and then performs attention and upsampling. However, upsampling is a coarse operation and cannot effectively restore important details. TCFormer [54] is similar to Clustered Attention, with the main difference being that it uses KNN to merge neighboring pixels to obtain sparse $\mathbf{Q}$, while Clustered Attention uses k-means to achieve sparse $\mathbf{Q}$. NLSA [37] utilizes pixel hash values to group pixels with the same hash into one group and then performs standard attention within each group. On the one hand, hash-based methods may result in hash collisions, leading to inaccurate groupings. On the other hand, NLSA also enforces group size uniformity, which can lead to similar pixels being placed in adjacent blocks, a situation that NLSA does not address. We address this issue in IASA by allowing the $\mathbf{Q}$ of each group to attend to $\mathbf{K}$ and $\mathbf{V}$ of adjacent groups.

As shown, these methods actually obtains slightly poor performance than ours. The reason lies in component of TAB. Specifically, Content-Aware Token Aggregation module computes the similarity between tokens and token centers rather than relying on hashing, thereby enhancing the accuracy of grouping. IASA performs attention among content-similar tokens to achieve more refined information interaction, complementing the information from IRCA.

Effects of Fusion Approach. We evaluate the impact of fusion methods for IASA and IRCA on performance. In the first model, we add the two output features together, while in the second model, we concatenate the two output features. As shown in Tab. 5, the addition method achieves the best performance with a PSNR improvement of 0.03dB∼0.09dB while maintaining lower complexity. These experimental results indicate that adding the output features together is more efficient and lightweight than concatenating them.

More analysis. In the supplementary material, we provide more ablation studies and analysis.

4.4. Visualization Analysis

To better understand the improvement brought by the TAB, we utilize LAM [13] to visualize the effective receptive field of an input patch. As shown in Fig. 5, with the assistance of the TAB, our CATANet (w/ TAB) benefits from more useful long-range token information compared to the first model (w/o TAB). Additionally, we compared our model with the CNN-based method RCAN [60] and the window-based attention method SwinIR-light [24]. The LAM map again

Table 6. Parameter, Multi-Adds, and Running Time comparison for scale factor ×4. CATANet-L(w/o $\mathcal{S}$) indicates CATANet-L without dividing token groups $\mathcal{G}$ into subgroups $\mathcal{S}$. The test input image size is $3\times256\times256$. The best and second best results are colored with red and blue, respectively.

Model	Params	Multi-Adds	Time
SwinIR-light [24]	897K	60.3G	158.1ms
SRFormer-light [64]	873K	56.5G	220.1ms
ATD-L [57]	494K	30.0G	144.2ms
SPIN [56]	555K	48.4G	435ms
CATANet-L(w/o $\mathcal{S}$)	535K	46.8G	188ms
CATANet-L (ours)	535K	46.8G	86ms

Table 7. PSNR comparison between our CATANet-L/M/S and other lightweight methods for scale factor ×2. † indicates being trained on DF2K [41].

Method	Params	Set5	Set14	B100	Urban100
ATD-L [57]	484K	38.23	33.94	32.33	32.95
SMFANet+ [63]	480K	38.18	33.82	32.28	32.64
CATANet-L (ours)	477K	38.28	33.99	32.37	33.09
ATD-M [57]	300K	38.14	33.78	32.26	32.58
DITN-Tiny [30]	367K	38.00	33.70	32.16	32.08
CATANet-M (ours)	306K	38.17	33.94	32.29	32.67
ATD-S [57]	229K	38.07	33.67	32.20	32.29
SAFMN [40]	228K	38.00	33.54	32.16	31.84
SeemoRe-T [52]†	220K	38.06	33.65	32.23	32.22
CATANet-S (ours)	230K	38.13	33.80	32.25	32.50

demonstrates that the TAB captures more long-range information and achieves a larger receptive field. These experimental results further demonstrate the advantages of TAB.

4.5. Model Size and Running Time Analyses

To demonstrate the effectiveness and efficiency of CATANet, we design three variants with different model size (S/M/L) and evaluate their PSNR results and inference speed.

Model Size In Fig. 1 and Tab. 7, we compare the performance and complexity of our CATANet-L/M/S with other lightweight SR methods, where ATD-light [57] is rescaled to similar model sizes as our three models denoted by ATD-S, ATD-M, and ATD-L. The results show that our CATANet-L/M/S achieves higher PSNR than other lightweight methods at each model size. Specifically, CATANet-M outperforms DITN-Tiny a large margin 0.59dB with fewer than 60K parameters and CATANet-S outperforms SeemoRe-T with a maximum PSNR improvement of 0.28 dB, even though SeemoRe-T was trained on a larger dataset.

Running Time To reduce the accidental error, we run each model 100 times on one RTX 4090 GPU and calculate the average time as the final running time. As shown in the Tab. 6, our CATANet-L achieves the fastest peed. Compared to the window-based methods SwinIR-light [24] and SRFormer-light [64], our CATANet-L achieves approximately double their speed. Compared to SPIN, which relies on token aggregation, CATANet benefits from our proposed efficient Content-Aware Token Aggregation, resulting in a significantly faster runtime, approximately five times faster than SPIN. Compared to ATD-L, which performs multiple
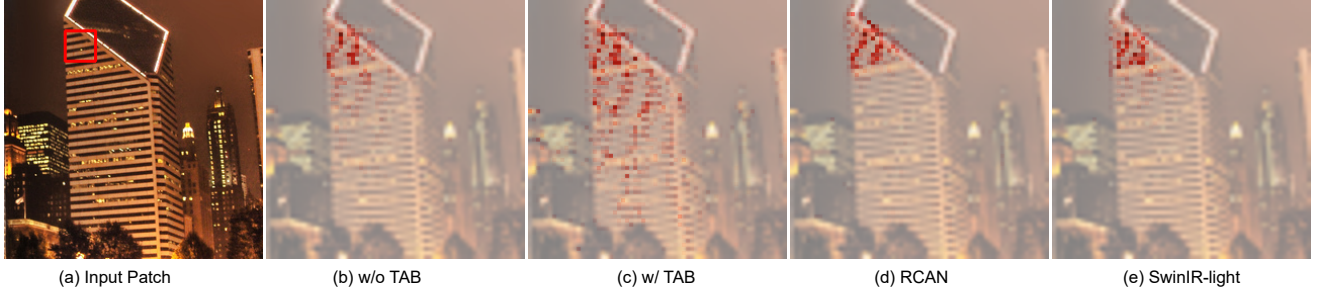
Figure 5. LAM Comparison: the variant without TAB (w/o TAB), the full CATANet (w/ TAB), RCAN and SwinIR-light for ×4 SR.
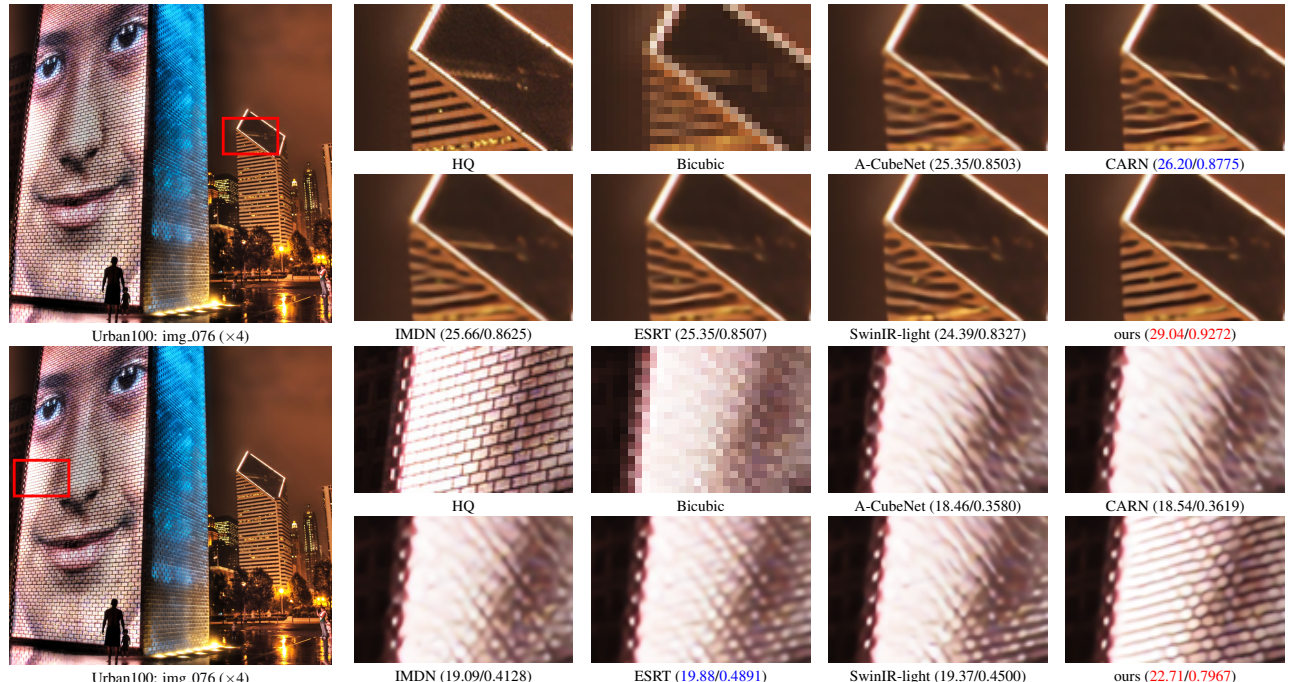

Figure 6. Visual comparisons of CATANet and other state-of-the-art lightweight SR methods. Metrics (PSNR/SSIM) are calculated on each patch. Best and second best results are colored with red and blue, respectively.

types of attention in parallel, increasing the computational burden, our CATANet-L achieves approximately $1.5\times$ the speed. Additionally, we also compared CATANet-L and CATANet-L without dividing the token groups $\mathcal{G}$ into subgroups $\mathcal{S}$, and CATANet-L is nearly 2 times faster.

5. Conclusion

In this paper, we propose a novel Lightweight Image Super-Resolution network called CATANet, which leverages token centers to aggregation content-similar tokens into content-aware regions. Specifically, the core component of CATANet is Token-Aggregation Block. Token-Aggregation Block is mainly comprised of Content-Aware Token Aggregation (CATA), Intra-Group Self-Attention, and Inter-Group Cross-Attention. CATA module efficiently aggregate similar tokens together, forming content-Aware regions. Intra-Group Self-Attention is responsible for fine-grained long-range information interaction within content-

aware regions. At the same time, we introduce Inter-Group Cross-Attention, which applies cross-attention between each group and token centers to further enhance global information interaction. We have presented extensive experimental results on various benchmark datasets, and our method has achieved superior performance while maintaining high inference efficiency in Lightweight Image Super Resolution.

Acknowledgments

References

[1] Namhyuk Ahn, Byungkon Kang, and Kyung-Ah Sohn. Fast, accurate, and lightweight super-resolution with cascading residual network. In *Proceedings of the European conference on computer vision (ECCV)*, pages 252–268, 2018. 5, 6

[2] Marco Bevilacqua, Aline Roumy, Christine Guillemot, and Marie-line Alberi Morel. Low-complexity single-image super-resolution based on nonnegative neighbor embedding. In *Procedings of the British Machine Vision Conference 2012*, 2012. 5

[3] Qiang Chen, Qiman Wu, Jian Wang, Qinghao Hu, Tao Hu, Errui Ding, Jian Cheng, and Jingdong Wang. Mixformer: Mixing features across windows and dimensions. In *Proceedings of the IEEE/CVF conference on computer vision and pattern recognition*, pages 5249–5259, 2022. 1

[4] Xiangyu Chen, Xintao Wang, Jiantao Zhou, Yu Qiao, and Chao Dong. Activating more pixels in image super-resolution transformer. In *Proceedings of the IEEE/CVF Conference on Computer Vision and Pattern Recognition (CVPR)*, pages 22367–22377, 2023. 1

[5] Zheng Chen, Yulun Zhang, Jinjin Gu, Linghe Kong, Xin Yuan, et al. Cross aggregation transformer for image restoration. *Advances in Neural Information Processing Systems*, 35:25478–25490, 2022. 1

[6] Zheng Chen, Yulun Zhang, Jinjin Gu, Linghe Kong, Xiaokang Yang, and Fisher Yu. Dual aggregation transformer for image super-resolution. In *Proceedings of the IEEE/CVF international conference on computer vision*, pages 12312–12321, 2023. 3

[7] Guoan Cheng, Ai Matsune, Qiuyu Li, Leilei Zhu, Huaijuan Zang, and Shu Zhan. Encoder-decoder residual network for real super-resolution. In *2019 IEEE/CVF Conference on Computer Vision and Pattern Recognition Workshops (CVPRW)*, 2019. 3

[8] Mingyu Ding, Bin Xiao, Noel Codella, Ping Luo, Jingdong Wang, and Lu Yuan. Davit: Dual attention vision transformers. In *Computer Vision–ECCV 2022: 17th European Conference, Tel Aviv, Israel, October 23–27, 2022, Proceedings, Part XXIV*, pages 74–92. Springer, 2022. 1

[9] Chao Dong, Chen Change Loy, Kaiming He, and Xiaoou Tang. Learning a deep convolutional network for image super-resolution. In *Computer Vision–ECCV 2014: 13th European Conference, Zurich, Switzerland, September 6-12, 2014, Proceedings, Part IV 13*, pages 184–199. Springer, 2014. 1, 2, 3

[10] Chao Dong, Chen Change Loy, and Xiaoou Tang. Accelerating the super-resolution convolutional neural network. In *Computer Vision–ECCV 2016: 14th European Conference, Amsterdam, The Netherlands, October 11-14, 2016, Proceedings, Part II 14*, pages 391–407. Springer, 2016. 1

[11] Xiaoyi Dong, Jianmin Bao, Dongdong Chen, Weiming Zhang, Nenghai Yu, Lu Yuan, Dong Chen, and Baining Guo. Cswin transformer: A general vision transformer backbone with cross-shaped windows. In *Proceedings of the IEEE/CVF conference on computer vision and pattern recognition*, pages 12124–12134, 2022. 2

[12] Alexey Dosovitskiy, Lucas Beyer, Alexander Kolesnikov, Dirk Weissenborn, Xiaohua Zhai, Thomas Unterthiner, Mostafa Dehghani, Matthias Minderer, Georg Heigold, Sylvain Gelly, et al. An image is worth 16x16 words: Transformers for image recognition at scale. *arXiv preprint arXiv:2010.11929*, 2020. 1

[13] Jinjin Gu and Chao Dong. Interpreting super-resolution networks with local attribution maps. In *Proceedings of the IEEE/CVF Conference on Computer Vision and Pattern Recognition*, pages 9199–9208, 2021. 7

[14] Yucheng Hang, Qingmin Liao, Wenming Yang, Yupeng Chen, and Jie Zhou. Attention cube network for image restoration. In *Proceedings of the 28th ACM international conference on multimedia*, pages 2562–2570, 2020. 5, 6

[15] Yanting Hu, Jie Li, Yuanfei Huang, and Xinbo Gao. Channel-wise and spatial feature modulation network for single image super-resolution. *IEEE Transactions on Circuits and Systems for Video Technology*, 30(11):3911–3927, 2019. 3

[16] Jia-Bin Huang, Abhishek Singh, and Narendra Ahuja. Single image super-resolution from transformed self-exemplars. In *2015 IEEE Conference on Computer Vision and Pattern Recognition (CVPR)*, 2015. 5

[17] Zheng Hui, Xiumei Wang, and Xinbo Gao. Fast and accurate single image super-resolution via information distillation network. In *Proceedings of the IEEE conference on computer vision and pattern recognition*, pages 723–731, 2018. 3

[18] Zheng Hui, Xinbo Gao, Yunchu Yang, and Xiumei Wang. Imdn. In *Proceedings of the 27th ACM International Conference on Multimedia*, 2019. 3, 5, 6

[19] Varun Jampani, Deqing Sun, Ming-Yu Liu, Ming-Hsuan Yang, and Jan Kautz. Superpixel sampling networks. In *Proceedings of the European Conference on Computer Vision (ECCV)*, pages 352–368, 2018. 2, 3

[20] Xiangtao Kong, Hengyuan Zhao, Yu Qiao, and Chao Dong. Classsr: A general framework to accelerate super-resolution networks by data characteristic. In *2021 IEEE/CVF Conference on Computer Vision and Pattern Recognition (CVPR)*, 2021. 1

[21] Zhen Li, Jinglei Yang, Zheng Liu, Xiaomin Yang, Gwanggil Jeon, and Wei Wu. Feedback network for image super-resolution. In *2019 IEEE/CVF Conference on Computer Vision and Pattern Recognition (CVPR)*, 2019.

[22] Zheyuan Li, Yingqi Liu, Xiangyu Chen, Haoming Cai, Jinjin Gu, Yu Qiao, and Chao Dong. Blueprint separable residual network for efficient image super-resolution. In *Proceedings of the IEEE/CVF conference on computer vision and pattern recognition*, pages 833–843, 2022. 1

[23] Zheyuan Li, Yingqi Liu, Xiangyu Chen, Haoming Cai, Jinjin Gu, Yu Qiao, and Chao Dong. Blueprint separable residual network for efficient image super-resolution. In *Proceedings of the IEEE/CVF conference on computer vision and pattern recognition*, pages 833–843, 2022. 3

[24] Jingyun Liang, Jiezhang Cao, Guolei Sun, Kai Zhang, Luc Van Gool, and Radu Timofte. Swinir: Image restoration using swin transformer. In *Proceedings of the IEEE/CVF inter-*

national conference on computer vision, pages 1833–1844, 2021. 1, 2, 3, 4, 5, 6, 7

[25] Bee Lim, Sanghyun Son, Heewon Kim, Seungjun Nah, and Kyoung Mu Lee. Enhanced deep residual networks for single image super-resolution. In *2017 IEEE Conference on Computer Vision and Pattern Recognition Workshops (CVPRW)*, 2017. 1, 3

[26] Bee Lim, Sanghyun Son, Heewon Kim, Seungjun Nah, and Kyoung Mu Lee. Enhanced deep residual networks for single image super-resolution. In *Proceedings of the IEEE conference on computer vision and pattern recognition workshops*, pages 136–144, 2017. 6

[27] Jie Liu, Jie Tang, and Gangshan Wu. Residual feature distillation network for lightweight image super-resolution. In *Computer Vision–ECCV 2020 Workshops: Glasgow, UK, August 23–28, 2020, Proceedings, Part III 16*, pages 41–55. Springer, 2020. 3, 4, 5, 6

[28] Jie Liu, Chao Chen, Jie Tang, and Gangshan Wu. From coarse to fine: Hierarchical pixel integration for lightweight image super-resolution. In *Proceedings of the AAAI Conference on Artificial Intelligence*, pages 1666–1674, 2023. 5

[29] Pengju Liu, Hongzhi Zhang, Kai Zhang, Liang Lin, and Wangmeng Zuo. Multi-level wavelet-cnn for image restoration. In *2018 IEEE/CVF Conference on Computer Vision and Pattern Recognition Workshops (CVPRW)*, 2018. 3

[30] Yong Liu, Hang Dong, Boyang Liang, Songwei Liu, Qingji Dong, Kai Chen, Fangmin Chen, Lean Fu, and Fei Wang. Unfolding once is enough: A deployment-friendly transformer unit for super-resolution. In *Proceedings of the 31st ACM International Conference on Multimedia*, pages 7952–7960, 2023. 7

[31] Ze Liu, Yutong Lin, Yue Cao, Han Hu, Yixuan Wei, Zheng Zhang, Stephen Lin, and Baining Guo. Swin transformer: Hierarchical vision transformer using shifted windows. In *Proceedings of the IEEE/CVF international conference on computer vision*, pages 10012–10022, 2021. 1, 3

[32] Zhisheng Lu, Juncheng Li, Hong Liu, Chaoyan Huang, Linlin Zhang, and Tieyong Zeng. Transformer for single image super-resolution. In *Proceedings of the IEEE/CVF conference on computer vision and pattern recognition*, pages 457–466, 2022. 5, 6

[33] Xiaotong Luo, Yuan Xie, Yulun Zhang, Yanyun Qu, Cuihua Li, and Yun Fu. Latticenet: Towards lightweight image super-resolution with lattice block. In *Computer Vision–ECCV 2020: 16th European Conference, Glasgow, UK, August 23–28, 2020, Proceedings, Part XXII 16*, pages 272–289. Springer, 2020. 5

[34] Xiaojiao Mao, Chunhua Shen, and Yu-Bin Yang. Image restoration using very deep convolutional encoder-decoder networks with symmetric skip connections. *Advances in neural information processing systems*, 29, 2016. 3

[35] D. Martin, C. Fowlkes, D. Tal, and J. Malik. A database of human segmented natural images and its application to evaluating segmentation algorithms and measuring ecological statistics. In *Proceedings Eighth IEEE International Conference on Computer Vision. ICCV 2001*, 2002. 5

[36] Yusuke Matsui, Kota Ito, Yuji Aramaki, Azuma Fujimoto, Toru Ogawa, Toshihiko Yamasaki, and Kiyoharu Aizawa. Sketch-based manga retrieval using manga109 dataset. *Multimedia Tools and Applications*, page 21811–21838, 2017. 5

[37] Yiqun Mei, Yuchen Fan, and Yuqian Zhou. Image super-resolution with non-local sparse attention. In *Proceedings of the IEEE/CVF conference on computer vision and pattern recognition*, pages 3517–3526, 2021. 4, 6, 7

[38] Aurko Roy, Mohammad Saffar, Ashish Vaswani, and David Grangier. Efficient content-based sparse attention with routing transformers. *Transactions of the Association for Computational Linguistics*, 9:53–68, 2021. 4

[39] Wenzhe Shi, Jose Caballero, Ferenc Huszar, Johannes Totz, Andrew P. Aitken, Rob Bishop, Daniel Rueckert, and Zehan Wang. Real-time single image and video super-resolution using an efficient sub-pixel convolutional neural network. In *2016 IEEE Conference on Computer Vision and Pattern Recognition (CVPR)*, 2016. 3, 4

[40] Long Sun, Jiangxin Dong, Jinhui Tang, and Jinshan Pan. Spatially-adaptive feature modulation for efficient image super-resolution. In *Proceedings of the IEEE/CVF International Conference on Computer Vision*, pages 13190–13199, 2023. 7

[41] Radu Timofte, Eirikur Agustsson, Luc Van Gool, Ming-Hsuan Yang, and Lei Zhang. Ntire 2017 challenge on single image super-resolution: Methods and results. In *Proceedings of the IEEE conference on computer vision and pattern recognition workshops*, pages 114–125, 2017. 5, 7

[42] Ashish Vaswani, Noam Shazeer, Niki Parmar, Jakob Uszkoreit, Llion Jones, Aidan N Gomez, Łukasz Kaiser, and Illia Polosukhin. Attention is all you need. *Advances in neural information processing systems*, 30, 2017. 1, 5

[43] Apoorv Vyas, Angelos Katharopoulos, and François Fleuret. Fast transformers with clustered attention. *Advances in Neural Information Processing Systems*, 33:21665–21674, 2020. 6, 7

[44] Chaofeng Wang, Zheng Li, and Jun Shi. Lightweight image super-resolution with adaptive weighted learning network. *arXiv preprint arXiv:1904.02358*, 2019. 5, 6

[45] Hang Wang, Xuanhong Chen, Bingbing Ni, Yutian Liu, and Jinfan Liu. Omni aggregation networks for lightweight image super-resolution. In *Proceedings of the IEEE/CVF Conference on Computer Vision and Pattern Recognition*, pages 22378–22387, 2023. 1

[46] Wenhai Wang, Enze Xie, Xiang Li, Deng-Ping Fan, Kaitao Song, Ding Liang, Tong Lu, Ping Luo, and Ling Shao. Pyramid vision transformer: A versatile backbone for dense prediction without convolutions. In *2021 IEEE/CVF International Conference on Computer Vision (ICCV)*, 2021. 1

[47] Xintao Wang, Ke Yu, Shixiang Wu, Jinjin Gu, Yihao Liu, Chao Dong, Yu Qiao, and Chen Change Loy. Esrgan: Enhanced super-resolution generative adversarial networks. In *Proceedings of the European conference on computer vision (ECCV) workshops*, pages 0–0, 2018. 3

[48] Yang Wang and Tao Zhang. Osffnet: Omni-stage feature fusion network for lightweight image super-resolution. In *Proceedings of the AAAI Conference on Artificial Intelligence*, pages 5660–5668, 2024. 5, 6

10

[49] Z. Wang, A.C. Bovik, H.R. Sheikh, and E.P. Simoncelli. Image quality assessment: From error visibility to structural similarity. *IEEE Transactions on Image Processing*, page 600–612, 2004. 5

[50] Zhendong Wang, Xiaodong Cun, Jianmin Bao, Wengang Zhou, Jianzhuang Liu, and Houqiang Li. Uformer: A general u-shaped transformer for image restoration. In *2022 IEEE/CVF Conference on Computer Vision and Pattern Recognition (CVPR)*, 2022. 1

[51] Tan Yu, Gangming Zhao, Ping Li, and Yizhou Yu. Boat: Bilateral local attention vision transformer. *arXiv preprint arXiv:2201.13027*, 2022. 3, 4

[52] Eduard Zamfir, Zongwei Wu, Nancy Mehta, Yulun Zhang, and Radu Timofte. See more details: Efficient image super-resolution by experts mining. In *International Conference on Machine Learning*. PMLR, 2024. 3, 7

[53] Syed Waqas Zamir, Aditya Arora, Salman Khan, Munawar Hayat, Fahad Shahbaz Khan, and Ming-Hsuan Yang. Restormer: Efficient transformer for high-resolution image restoration. In *2022 IEEE/CVF Conference on Computer Vision and Pattern Recognition (CVPR)*, 2022. 1

[54] Wang Zeng, Sheng Jin, Wentao Liu, Chen Qian, Ping Luo, Wanli Ouyang, and Xiaogang Wang. Not all tokens are equal: Human-centric visual analysis via token clustering transformer. In *Proceedings of the IEEE/CVF Conference on Computer Vision and Pattern Recognition*, pages 11101–11111, 2022. 6, 7

[55] Roman Zeyde, Michael Elad, and Matan Protter. On single image scale-up using sparse-representations. In *Curves and Surfaces: 7th International Conference, Avignon, France, June 24-30, 2010, Revised Selected Papers 7*, pages 711–730. Springer, 2012. 5

[56] Aiping Zhang, Wenqi Ren, Yi Liu, and Xiaochun Cao. Lightweight image super-resolution with superpixel token interaction. In *International Conference on Computer Vision*, 2023. 2, 3, 4, 5, 6, 7

[57] Leheng Zhang, Yawei Li, Xingyu Zhou, Xiaorui Zhao, and Shuhang Gu. Transcending the limit of local window: Advanced super-resolution transformer with adaptive token dictionary. In *Proceedings of the IEEE/CVF Conference on Computer Vision and Pattern Recognition*, pages 2856–2865, 2024. 2, 7

[58] Xindong Zhang, Hui Zeng, and Lei Zhang. Edge-oriented convolution block for real-time super resolution on mobile devices. In *Proceedings of the 29th ACM International Conference on Multimedia*, 2021. 1

[59] Xindong Zhang, Hui Zeng, Shi Guo, and Lei Zhang. Efficient long-range attention network for image super-resolution. In *European conference on computer vision*, pages 649–667. Springer, 2022. 1, 3, 5, 6

[60] Yulun Zhang, Kunpeng Li, Kai Li, Lichen Wang, Bineng Zhong, and Yun Fu. Image super-resolution using very deep residual channel attention networks. In *Proceedings of the European conference on computer vision (ECCV)*, pages 286–301, 2018. 3, 7

[61] Yulun Zhang, Yapeng Tian, Yu Kong, Bineng Zhong, and Yun Fu. Residual dense network for image super-resolution. In *Proceedings of the IEEE conference on computer vision and pattern recognition*, pages 2472–2481, 2018. 1, 3

[62] Mingjun Zheng, Long Sun, Jiangxin Dong, and Jinshan Pan. Smfanet: A lightweight self-modulation feature aggregation network for efficient image super-resolution. In *ECCV*, 2024. 3

[63] Mingjun Zheng, Long Sun, Jiangxin Dong, and Jinshan Pan. Smfanet: A lightweight self-modulation feature aggregation network for efficient image super-resolution. In *European Conference on Computer Vision*, pages 359–375. Springer, 2025. 7

[64] Yupeng Zhou, Zhen Li, Chun-Le Guo, Song Bai, Ming-Ming Cheng, and Qibin Hou. Srformer: Permuted self-attention for single image super-resolution. In *Proceedings of the IEEE/CVF International Conference on Computer Vision*, pages 12780–12791, 2023. 5, 7